Catalysis Science & Technology

Accepted Manuscript

ROYAL SOCIETY OF CHEMISTRY

www.rsc.org/catalysis

CO oxidation on single and multilayer Pd oxides on Pd(111): Mechanistic insights from RAIRS

Feng Zhang[(a)], Tao Li[(a)], Li Pan[(b)], Aravind Asthagiri[(b)] and Jason F. Weaver[(a),*]

[(a)]Department of Chemical Engineering, University of Florida, Gainesville, FL 32611, USA

[(b)] William G. Lowrie Department of Chemical & Biomolecular Engineering, The Ohio State University, Columbus, OH 43210, USA

*To whom correspondence should be addressed, weaver@che.ufl.edu

Tel. 352-392-0869, Fax. 352-392-9513

Abstract

We investigated the oxidation of CO on the Pd_5O_4 surface oxide and a multilayer PdO(101) film on Pd(111) using direct, isothermal rate measurements, reflection absorption infrared spectroscopy (RAIRS) and density functional theory calculations. Our results show that the PdO(101) film is intrinsically more reactive than the surface oxide toward CO oxidation, and that the reaction kinetics occurs autocatalytically on both oxides, with the rate of CO_2 production increasing as the oxides are reduced. The RAIRS measurements reveal that self-accelerating reaction kinetics occurs on PdO(101) because oxide reduction generates both oxygen vacancies within PdO(101) domains as well as Pd(111) domains. These reduced structures bind CO more strongly than the pristine PdO(101) surface, causing the CO surface concentration and thus the reaction rate to increase as the oxide is progressively reduced by reaction. In contrast, we find that reduction of the surface oxide generates only Pd(111) domains which bind CO strongly and sustain reaction.

The surface chemistry of late transition metal oxides plays an important role in many applications of oxidation catalysis. Under sufficiently oxygen-rich conditions, metal oxide layers can form on the surface of a metallic catalyst and usually cause significant changes in catalyst performance because the surface chemical properties of metals and metal oxides can be quite different. The importance of metal oxide formation in the catalytic oxidation of CO over late transition metals (e.g., Ru, Pd, Pt, Rh) has been widely discussed in the literature,[1-13] with this work being motivated largely by observations that late transition metals tend to become highly active toward CO oxidation under conditions where oxide structures start to develop on the surface. For example, Goodman and coworkers have reported detailed investigations of CO oxidation on several crystalline metal surfaces based on reaction rate measurements and *in situ* surface IR spectroscopy, which can allow identification of distinct surface phases at millibar pressures.[14-17] Their work reveals three kinetic regimes for the oxidation of CO over transition-metal surfaces as a function of the O_2:CO ratio in the gas-phase, namely, a CO-inhibited regime, a transitory CO-uninhibited regime and a regime in which metal oxide layers cover the surface. Of particular interest has been the transitory regime in which the CO oxidation rate exhibits an abrupt increase when the system switches from a condition at which adsorbed CO inhibits reaction to one in which the surface becomes oxygen-rich and metal oxide structures begin to form.

In situ measurements that probe the surface structure during reaction have indeed provided strong evidence that CO oxidation rates increase when metal oxide layers develop on late transition-metal surfaces,[4, 6, 8, 9, 18-25] particularly when so-called two-dimensional (2D) oxides[26] form prior to the bulk oxides. Among Pd surfaces, the Pd(100) surface has been the most widely investigated using *in situ* methods and several investigations show that increases in the CO

oxidation activity of the Pd(100) surface coincide with the formation of a well-ordered 2D Pd oxide ($\sqrt{5} \times \sqrt{5}$ R27°)[9, 18, 19, 27] where the $\sqrt{5}$ oxide resembles a slightly distorted, single layer of PdO(101).[28, 29] A recent investigation combining surface X-ray diffraction (SXRD) with product detection further shows that bulk-like PdO(101) layers develop on Pd(100) at near ambient pressure conditions and are also highly active toward CO oxidation.[9] Lastly, Toyoshima et al.[30] have recently studied CO oxidation on Pd(111) using high pressure X-ray photoelectron spectroscopy (HP-XPS) and find that Pd(111) also exhibits an increase in CO oxidation activity when thin metal-oxide layers form on the surface.

These prior studies demonstrate that metal oxide layers can have an important influence on the catalytic oxidation of CO on Pd surfaces and other transition metals under realistic reaction conditions. However, several details of the reaction mechanisms remain unclear. For example, both computational[25, 31] and ultrahigh vacuum (UHV) studies[32-38] suggest that facile CO oxidation occurs either within metal domains that co-exist with 2D oxide structures or at the edges of oxide islands, and that direct reaction of CO at the 2D oxide surface is much slower by comparison. Such information can be difficult to obtain from *in situ* studies, yet is essential for developing an accurate mechanistic description of the surface reaction kinetics. Furthermore, in many *in situ* investigations, the measured CO oxidation rate has been limited by the rate of gaseous CO transport to the surface, and consequently measurements performed under such mass-transport limitations have been unable to provide a quantitative comparison of the reactivity of different surface oxygen phases, particularly single layer vs. multilayer oxides.[9, 39]

Surface science investigations with well-defined oxide structures can provide key mechanistic insights for understanding CO oxidation on the metal oxides layers that develop on transition-metal surfaces under realistic reaction conditions as well as information needed to

develop atomic-level descriptions of the reaction kinetics. The importance of investigating structurally well-defined oxide layers may be seen from the few prior investigations of CO oxidation on Pd(111) that have been reported. Gabasch et al. report that the reactivity of Pd-O species toward CO oxidation diminishes with increasing oxidation state.[33] Specifically, those researchers find that chemisorbed oxygen atoms are more reactive than 2D oxide layers that form on Pd(111) in isothermal CO oxidation experiments performed in UHV, and that a more fully oxidized Pd(111) film on a NiAl surface exhibits a significantly lower activity than the 2D oxides. In contrast, a prior surface science investigation shows that CO oxidation is highly facile on a multilayer PdO(101) film grown on Pd(111),[40] in excellent agreement with predictions of DFT.[41] A likely explanation for these seemingly conflicting results is that the bulk-like Pd oxide which formed on the NiAl surface is structurally dissimilar from PdO(101), and, as noted by Gabasch et al,[33] exposes a minimal concentration of coordinatively unsaturated sites. Importantly, recent *in situ* SXRD and HP-XPS measurements show that an epitaxial, multilayer PdO(101) thin film forms on Pd surfaces under semi-realistic reaction conditions (i.e., millibar pressures),[9, 23] thereby supporting the view that UHV experiments with PdO(101) thin films can provide insights that are relevant for understanding applications of oxidation catalysis by Pd.

In the present study, we performed direct, isothermal rate measurements and reflection absorption infrared spectroscopy (RAIRS) to investigate CO oxidation on the well-defined 2D Pd_5O_4 oxide and a multilayer PdO(101) film grown on Pd(111) in ultrahigh vacuum (UHV). This study is the first to provide a direct comparison of the CO oxidation behavior on these ultrathin oxide layers on Pd(111). Our results reveal differences in the mechanistic aspects as well as the intrinsic reactivity of the single layer Pd_5O_4 oxide vs. the PdO(101) film toward CO oxidation.

Of particular significance is our finding that the creation of oxygen-vacancies in the PdO(101) surface promotes CO oxidation on the multilayer oxide.

The evolution of oxygen phases on Pd(111) has been extensively investigated. Oxygen atoms initially chemisorb onto the Pd(111) surface and arrange into a p(2×2) structure up to 0.25 ML (monolayer). After the chemisorbed layer saturates, crystalline 2D oxide phases, so-called "surface oxides", develop and saturate at an oxygen coverage near 0.70 ML. Several meta-stable 2D oxides can form on Pd(111) below 600 K,[42] but transform to the preferred 2D Pd_5O_4 oxide above 600 K.[43, 44] Increasing the oxygen coverage above 0.70 ML results in the formation of PdO seeds that grow into a multilayer PdO(101) film as oxidation progresses.[45, 46] At moderate temperature, a high-quality, conformal PdO(101) film forms on Pd(111) and effectively saturates at an oxygen coverage between 3 and 4 ML, which is equal to a thickness of 4 to 5 oxide layers.

Figure 1 shows model representations of the 2D Pd_5O_4 oxide and PdO(101) surfaces investigated in this study. The structures of both of these oxides have been characterized extensively in prior studies.[21, 26, 42, 43, 47] The Pd_5O_4 oxide has a square unit cell with side lengths equal to √6 times that of the Pd(111) lattice constant, and will henceforth be referred to as the √6 oxide.[44] Each unit cell contains four 2-fold coordinated Pd atoms and one 4-fold coordinated Pd atom as well as both 3-fold and 4-fold coordinated oxygen atoms. The total oxygen density in the √6 oxide is 0.67 ML where we define 1 ML (monolayer) as equal to the surface atom density of Pd(111). The √6 oxide forms a large commensurate unit cell with the Pd(111) substrate, as depicted in Figure 1a, and the structure of the √6 oxide bears no resemblance to any lattice plane of bulk PdO. The stoichiometric PdO(101) surface is characterized by a rectangular unit cell and is comprised of alternating rows of 3-fold (3f) and 4-fold (4f) coordinated Pd atoms and O atoms, where the 3f atoms are referred to as coordinatively unsaturated (cus) since these atoms are

missing a bonding partner compared with the bulk atoms of PdO (Figure 1b). The areal density of each type of coordinatively distinct atom of the PdO(101) surface is equal to 35% of the atomic density of the Pd(111) surface. Hence, the coverage of cus-Pd atoms is equal to 0.35 ML, and each PdO(101) layer contains 0.7 ML of Pd atoms and 0.7 ML of O-atoms.

We investigated the oxidation of CO on the √6 oxide and a PdO(101) thin film under isothermal conditions using direct measurements of the CO_2 production rate. We prepared the oxide layers for these experiments following previously-reported procedures in which we oxidize clean Pd(111) using plasma-generated O-atom beams.[46] We estimate oxygen coverages using O_2 temperature programmed desorption (TPD) and used low energy electron diffraction (LEED) to confirm that the desired oxide structures are generated. We investigated a PdO(101) film initially containing about 3.5 ML of oxygen atoms, while the √6 oxide saturates at an oxygen coverage of about 0.7 ML.

For the rate measurements, we maintain the oxides at a constant surface temperature and introduce a constant partial pressure of CO (5×10^{-9} Torr) into the UHV chamber while simultaneously monitoring the CO_2 partial pressure using a mass spectrometer. At temperatures between 400 K and 500 K, the gaseous CO completely consumes the oxides and causes CO_2 to evolve in measurable quantities as a function of time. Because the CO_2 partial pressure is proportional to the CO_2 desorption rate in a well-pumped system, these experiments provide a direct and continuous measure of the CO oxidation rate as the reaction consumes oxygen at the (initially) oxide surfaces. Here, we present data only for experiments conducted at 450 K as we find that this temperature is optimal for continuously oxidizing CO on both oxide surfaces at the CO partial pressure studied.

We also report results of density functional theory (DFT) calculations which were performed using the Vienna *ab initio* simulation package (VASP)[48, 49] with projected augmented wave (PAW) pseudopotentials provided in the VASP database.[50, 51] The Perdew-Burke-Ernzerhof (PBE) exchange-correlation functional[52] with a plane wave cutoff of 400 eV was used. The PdO(101) surface was modeled by a 4 × 1 rectangular unit cell, where the $\vec{a}$ and $\vec{b}$ vectors denote [010] and [$\bar{1}$01] directions, respectively, with a 4 × 2 × 1 Monkhorst-Pack *k*-point mesh. The PdO slab was modeled with four layers, which is equivalent to a 9 Å thick slab. The bottom layer is fixed with the rest of the atoms allowed to relax until the forces are less than 0.03eV/ Å. A vacuum spacing of 20 Å is introduced, which is sufficient to eliminate any spurious interactions along the surface normal. As discussed in prior studies,[53-59] the model slab is strained (a = 3.057 Å, b = 6.352 Å) to match the previously-reported structure of the PdO(101) film as determined from LEED experiments.[47] Vibrational frequencies were calculated using finite difference methods within the harmonic approximation. The frequencies for CO on the surface are obtained from relaxed configurations, but with the surface fixed for the frequency calculation. The obtained CO stretch frequencies were corrected by scaling with a factor of 1.024 which is the ratio of the experimental harmonic gas phase C-O stretch frequency (2170 cm^{-1}) and the corresponding calculated value (2120 cm^{-1}) in PBE.

Figure 2 shows CO_2 production rate curves obtained during the oxidation of CO on the √6 oxide and the PdO(101) film at 450 K. For comparison, we also show a CO_2 production rate curve obtained from Pd(111) initially covered with 0.21 ML of oxygen atoms for a surface temperature of 450 K. For both oxides, the CO oxidation rate increases abruptly when CO is introduced into the chamber (t = 0), and then increases more slowly with time. After rising to a maximum, the reaction rate drops back to the baseline as oxygen is depleted from the surface.

The initial reaction rates are equivalent to the rates of CO oxidation on the pristine oxide surfaces for the conditions studied, while the rates change with time after the initial increase due to changes in the surface structure and binding sites that occur as the oxides are reduced by reaction.

As seen in Figure 2, the initial reaction rate is larger on PdO(101) compared with the √6 oxide, thus demonstrating that the pristine PdO(101) surface is more reactive than the √6 oxide toward CO oxidation when reaction occurs directly on the oxide surfaces in the absence of O_2. The initial CO oxidation rate is about seven times larger for the PdO(101) film compared with the √6 oxide for reaction at 450 K and a CO partial pressure of 5×10^{-9} Torr, with initial rates equal to ~0.040 ML/min vs. 0.006 ML/min. The initial reaction rate is also higher for the PdO(101) film vs. the √6 oxide in direct rate measurements performed at 400 K and 500 K. These results demonstrate clearly that the pristine PdO(101) surface is intrinsically more reactive that the √6 oxide surface toward CO oxidation.

The CO oxidation kinetics is autocatalytic on both the PdO(101) film and the √6 oxide in that the reaction rate increases toward a maximum as reaction progresses. The autocatalytic behavior indicates generally that the creation of reduced sites on the surface promotes further CO oxidation, and thus causes the reaction rates to increase as the oxides are reduced. The decline in reaction rate near the end of the measurements occurs when the supply of oxygen becomes rate limiting. While CO oxidation is autocatalytic on both oxides, the kinetics exhibits distinct characteristics for the PdO(101) film vs. the √6 oxide, with reaction on the √6 oxide being more strongly autocatalytic. At the start of the measurement, the reaction rate on the √6 oxide rises to a small value (~0.006 ML/min) and remains relatively steady for about five minutes. The rate then begins to increase sharply with increasing time until reaching a maximum value of 0.071 ML/min after about 18 minutes. In fact, we find that the increase of the reaction rate with time is

well approximated as exponential growth for the √6 oxide. For the data shown in Figure 2, the reaction rate on the √6 oxide increases by more than a factor of 12 from the start of the reaction to the maximum rate. Gabasch et al. have also reported that CO oxidation on 2D oxide layers on Pd(111) occurs autocatalytically,[33] and noted that reduced sites in the oxide structure appear to promote reaction. In the present study, the reaction rate on the √6 oxide increases by a greater amount as reaction progresses compared with previous work.[33] This difference most likely indicates that the √6 oxide studied here has fewer defects than that investigated previously.

Compared with the √6 oxide, the CO oxidation rate on the PdO(101) film increases more slowly with time, and is well-approximated by a linear function for times between about 5 and 35 minutes. The reaction rate on the PdO(101) film reaches a maximum value of ~0.109 ML/min after 38 minutes of reaction, and the remaining oxygen coverage on the surface is ~0.51 ML at the rate maximum. The reaction rate on the PdO(101) film exhibits a less dramatic increase compared with the √6 oxide, increasing by a factor of 2.7 from the start of the measurement to the rate maximum. These characteristics suggest that the √6 oxide is significantly less reactive toward CO than are the reduced sites which are created as the √6 oxide is reduced, whereas, in comparison, the reactivity of the pristine PdO(101) surface is closer to that of the reduced sites that develop on this surface during reaction.

It is instructive to also compare the CO oxidation rates measured on the oxides with those found for chemisorbed O-atoms on Pd(111). The reaction rate curve obtained from the metal surface, initially covered with 0.21 ML of O-atoms, rises to an initial value of ~0.051 ML/min when CO is introduced into the chamber and then reaches a maximum of about 0.068 ML/min after 1.75 minutes. While these rates are higher than the initial CO oxidation rate on PdO(101), the maximum reaction rate reached on the PdO(101) film is higher than the maximum rate of CO

oxidation on the metal surface for the conditions studied. An implication is that the pristine PdO(101) surface is slightly less reactive than the metal surface, but that reduction of this oxide produces a surface that is more reactive than the metal toward CO oxidation. Also, the maximum reaction rate achieved on the √6 oxide is nearly identical to that reached on the metal surface, and occurs once the total oxygen coverage decreases to ~0.25 ML which is very close to the saturation coverage of the p(2×2) oxygen adlayer on Pd(111). Importantly, the reaction rates measured in the present study apply to conditions that deviate significantly from the steady-state, elevated pressure conditions that are employed in catalytic applications. In addition to operating at higher temperature and pressure, catalytic applications also involve the adsorption and dissociation of O_2 to regenerate catalytically-active surface oxygen phases. Further study is needed to determine how the concurrent regeneration of surface oxygen species via O_2 dissociation affects the CO oxidation kinetics on oxidized Pd(111), and thereby determine the relative reactivity of the √6 oxide vs. PdO(101) under steady state conditions.

We performed RAIRS measurements to characterize how the CO binding sites and oxide structures change during CO oxidation at 450 K. In a previous study, we found that the C-O stretching frequencies are highly sensitive to the local CO bonding environment on the √6 oxide and PdO(101) and provided assignments of the RAIRS peaks.[60] Thorough experiments by Farkas et al. also demonstrate the high sensitivity of RAIRS for identifying CO molecules adsorbed in different local environments on the RuO_2(110) surface.[61, 62] For the RAIRS experiments in this study, we conducted CO oxidation on the oxide layers at 450 K and intermittently discontinued the reaction to collect RAIR spectra. For the PdO(101) film, we allowed reaction to occur for 5 minutes at 450 K at a CO partial pressure of 5×10^{-9} Torr, followed by abruptly evacuating CO from the chamber and then cooling the sample to 95 K. After collecting an initial RAIR spectrum

("reaction" spectrum) at 95 K (Figure 3a), we saturated the surface with CO at 95 K and collected a second RAIR spectrum ("resaturation" spectrum, Figure 3b). The reaction spectrum provides information about the CO molecules that remain adsorbed at 450 K when the CO is evacuated from the chamber, while the resaturation spectrum provides information about the CO binding sites that are available on the surface, though not necessarily populated by CO at the reaction temperature. We repeated this process up to a cumulative reaction time of 60 min at 450 K. We followed the same procedure to characterize the √6 oxide, but allowed reaction to occur in 3 minute intervals. We note that a fraction of the CO adsorbed during the saturation step at 95 K reacts with the oxides during warming from 95 K to 450 K. Based on TPRS experiments performed with the oxides, we estimate that less than 0.20 ML of oxygen atoms was consumed during the warming step.

Figures 3a and 3b show the reaction and resaturation RAIR spectra obtained after performing CO oxidation on the PdO(101) film at 450 K, and the bottom trace in Figure 3b shows a reference RAIR spectrum obtained after saturating the initial PdO(101) surface with CO at 95 K. The reference spectrum exhibits an intense peak at 2135 cm^{-1} that arises from CO molecules adsorbed on top of cus-Pd sites of the pristine PdO(101) surface.[60] The reference spectrum also exhibits a small feature at about 2110 cm^{-1}, which is consistent with CO molecules adsorbed on atop sites of metallic Pd. The appearance of this feature suggests that the initial PdO(101) surface is partially reduced and exposes small quantities of metallic Pd nanoclusters.[63] The small feature at 1864 cm^{-1} is attributable to CO adsorbed on threefold hollow sites of Pd(111) facets, further supporting the conclusion that small metallic domains are present on the initial surface of the oxide. Lastly, the low spectral intensity between ~2000 and 1900 cm^{-1} indicates that negligible quantities of CO adsorb in bridging cus-Pd sites of PdO(101).

Figure 3a shows the "reaction" IR spectra obtained from PdO(101) at 95 K after performing consecutive reaction cycles at 450 K. Next to each spectrum, we show the cumulative time at which CO oxidation occurred on the surface at 450 K prior to the RAIRS measurement. We note, however, that additional CO oxidation occurs when the CO-saturated sample is warmed from 95 to 450 K and thus that the times listed in the figure do not exactly correspond to the reaction times in the continuous isothermal rate measurement (Figure 2). The reaction RAIR spectra exhibit two main features at ~2090 cm^{-1} and 1823 cm^{-1}, with intensities that change as reaction progresses. Notably, Gao and Goodman have reported IR peaks at 2087 and 2142 cm^{-1} during CO oxidation on Pd(100), Pd(111) and Pd(110) at millibar reactant pressures and oxygen-rich reaction conditions and suggested that a common oxide forms on these surfaces.[64] Our current results suggest that PdO(101) develops on each of the Pd surfaces studied by those authors. Recent *in situ* studies also show that a multilayer PdO(101) film develops on the Pd(100) surface under sufficiently oxidizing conditions.[9, 19] Our data shows that the peak at 2090 cm^{-1} is dominant during the early reaction period but decreases in intensity as reaction progresses, becoming immeasurable after the rate maximum is passed. The peak at 1837 cm^{-1} intensifies as reaction progresses and becomes the only observable peak in spectra collected beyond the rate maximum. Notably, the absence of a peak at 2135 cm^{-1} indicates that CO molecules adsorb in only small concentrations on pristine PdO(101) domains at 450 K. As such, it is reasonable to conclude that the CO molecules associated with the peaks at 2090 cm^{-1} and 1823 cm^{-1} are more strongly bound than atop-CO species on pristine PdO(101).

We attribute the peaks at ~2090 cm^{-1} and 1823 cm^{-1} to CO molecules adsorbed on PdO(101) domains vs. metallic Pd domains, respectively. The peak at 1823 cm^{-1} is consistent with low coverages of CO adsorbed in threefold hollow sites of Pd(111) facets. Experiments of CO

adsorption on clean Pd(111) demonstrate that CO molecules adsorb in hollow sites up to a coverage of 0.33 ML and organize into an ordered $\sqrt{3} \times \sqrt{3}$ R30° structure.[65] The IR peak for hollow-CO on Pd(111) blueshifts with increasing CO coverage, developing into a sharp peak at 1854 cm^{-1} once the layer orders into the $\sqrt{3} \times \sqrt{3}$ R30° structure.[66] Above 0.33 ML, the adsorbed CO molecules arrange into a c(4×2) structure on Pd(111) which saturates at a CO coverage of 0.50 ML.[67] A recent study shows that CO molecules bind in a mixture of bridge and hollow sites in the c(4×2) structure and that the IR spectrum obtained from this layer exhibits a major peak at about 1954 cm^{-1}.[60]

From DFT calculations, we find that atop-CO molecules on PdO(101) experience a significant increase in binding energy when adsorbed next to a cus-O atom vacancy vs. next to a cus-O atom. We will henceforth refer to these sites as Pd_{cus}/O_v and Pd_{cus}/O_{cus}, where O_v represents a cus-O atom vacancy in the PdO(101) surface. DFT predicts binding energies of ~133 vs. 215 kJ/mol for atop-CO on the Pd_{cus}/O_{cus} vs. Pd_{cus}/O_v sites, and normal mode analysis predicts C-O stretching frequencies of 2135 cm^{-1} and ~2095 cm^{-1} for low coverages of atop-CO on the Pd_{cus}/O_{cus} and Pd_{cus}/O_v sites, respectively, in very good agreement with the measured values. For comparison, our DFT calculations indicate that CO adsorbs most strongly on hollow sites of Pd(111) at low CO coverage, achieving a binding energy of about 200 kJ/mol. Thus, according to DFT, CO achieves slightly stronger, or at least similar, binding at the atop-Pd_{cus}/O_v site as it does on hollow sites of Pd(111). The reaction RAIR spectra obtained during isothermal CO oxidation on PdO(101) demonstrate that reduction of the PdO(101) film creates surface sites on which CO binds more strongly compared with adsorption on the pristine PdO(101) surface. As such, the surface concentration of CO should increase as reaction progresses, and thereby provide more opportunity for CO molecules to react with oxygen atoms at the oxide surface.

Figure 3b shows the resaturation IR spectra collected after saturating the partially-reduced PdO(101) surfaces at 95 K. In the early reaction period, the peak at 2135 cm^{-1} from atop-CO on pristine PdO(101) is dominant. A broad peak centered between 2070 and 2080 cm^{-1} and a sharp peak at 1964 cm^{-1} are also apparent in the resaturation spectra collected in the early reaction period, but are less intense than the peak at 2135 cm^{-1}. We attribute the broad feature between 2070 and 2080 cm^{-1} to atop-CO on Pd_{cus}/O_v sites, where this feature is redshifted compared with the peak obtained at low CO coverage. The peak at 1964 cm^{-1} is consistent with bridging CO species on Pd(111) domains which form at higher CO coverages. Notably, the atop-CO feature splits into two components centered at 2122 and 2140 cm^{-1} in the resaturation RAIR spectrum collected just prior to the rate maximum (Figure 3b). The peak at 2140 cm^{-1} likely originates from atop-CO on Pd_{cus}/O_{cus} sites of PdO(101), but the origin of the peak at 2122 cm^{-1} is not known.

In the resaturation RAIR spectra, the intensities of the atop-CO features at 2135 and ~2075 cm^{-1} both diminish as the CO oxidation rate increases to the maximum, demonstrating that PdO(101) surface sites are consumed by reaction. However, the features at 2135 and 2075 cm^{-1} persist even after CO abstracts a significant quantity of oxygen from the film, up to as much as ~3 ML of oxygen atoms. Considering that the cus-O atom concentration is only 0.35 ML at the PdO(101) surface, the presence of cus-Pd surface sites after prolonged reaction strongly suggests that PdO(101) surface domains are regenerated during CO oxidation at 450 K. Also, the intensity of the peak at 1964 cm^{-1} remains relatively constant in the resaturation RAIR spectra with increasing reaction time up to the rate maximum. This behavior further supports the idea that PdO(101) surface domains are regenerated during CO oxidation at 450 K, since otherwise the

fractional coverage of metallic domains, and other reduced phases, would be expected to increase as reaction progresses.

Features arising from CO adsorbed on metallic Pd structures intensify in the resaturation RAIR spectra obtained after passing the maximum reaction rate, at which point the total oxygen coverage has decreased to about 0.5 ML. The peak at 1964 cm^{-1} intensifies significantly and is the dominant feature in the resaturation RAIR spectra obtained after the rate maximum. Smaller features at 2109 and 2000 cm^{-1} are also evident in the resaturation RAIR spectra. As mentioned above, the feature at 2109 cm^{-1} is characteristic of CO adsorbed on atop sites of metallic Pd, and is typically observed when metallic Pd is present in the form of nanoclusters.[63] The peak at 2000 cm^{-1} is characteristic of CO adsorbed on metallic Pd(100)[68] or Pd(110)[69], so its appearance in the RAIR spectra suggests that Pd(100) and/or (110)-like domains develop during the reduction of PdO(101) films at 450 K. Overall, the evolution of the RAIR spectra reveal that the CO oxidation rate remains high when PdO(101) surface domains are present, and increases autocatalytically due to the generation of both Pd(111) domains and O_v sites in the PdO(101) surface domains.

Figures 4a and 4b show the reaction and resaturation RAIR spectra obtained for CO oxidation on the √6 oxide at 450 K, and the bottom trace in Figure 4b shows the reference RAIR spectrum for CO adsorbed to saturation on the √6 oxide at 95 K. Martin et al. have recently reported a detailed investigation of CO adsorption on the √6 oxide based on RAIRS, DFT and high-resolution core level spectroscopy (HRCLS).[60] These researchers find that CO achieves the highest binding energy (~97 kJ/mol) on the √6 oxide by adsorbing on so-called bridge-A sites (Figure 1), and assign the main RAIR peak at 2011 cm^{-1} to this bridging species. CO can also

bind on bridge-B and atop 2f sites of the √6 oxide (Figure 1), achieving binding energies of ~53 and 57 kJ/mol, respectively. DFT calculations suggest that CO on the bridge-B and atop 2f sites gives rise to the RAIR peaks at 1944 and 2126 cm^{-1}.[60] The small features at 2071, 2105 and 2112 cm^{-1} arise from CO adsorbed on the √6 oxide, but their precise origin is not known.

The reaction RAIR spectra obtained from the √6 oxide (Figure 4a) exhibit a single peak at 1823 cm^{-1} that intensifies with increasing reaction time. This peak is consistent with CO adsorbed on hollow sites of Pd(111), and thus the growth of the 1823 cm^{-1} peak demonstrates that the exposed area of Pd(111) increases as the √6 oxide is reduced during reaction with CO at 450 K. Moreover, the corresponding rapid increase in the reaction rate suggests that the creation of Pd(111) domains promotes the reaction of CO with the √6 oxide, in agreement with conclusions made by Gabasch et al.[33] This finding is also consistent with prior studies of CO oxidation on Pd(100)[35] and Rh surfaces[6, 25, 32] in which reaction was concluded to occur either within O-covered metal domains that develop as the surface oxide is consumed by reaction or at the edges of 2D oxide islands. In these cases, the surface oxide acts as an oxygen source to sustain reaction and the CO oxidation rate is self-accelerating since the quantity of O-covered metallic domains and 2D oxide island edges increases as reaction progresses. Consistent with this interpretation, several DFT studies predict lower energy barriers for CO oxidation at the edge of a 2D oxide domain on a metal surface compared with reaction on the O-covered metal surface or the 2D oxide surface.[25, 70] Computational studies have also predicted that 2D oxide and metallic domains are likely to coexist at the temperature and pressure conditions at which high CO oxidation rates have been observed experimentally under semi-realistic conditions.[71-74]

The resaturation RAIR spectra obtained prior to the reaction rate maximum exhibit C-O stretching features that are characteristic of coexisting √6 oxide and Pd(111) domains. After

passing the rate maximum, the resaturation RAIR spectra only exhibit features that originate from CO adsorbed on metallic domains. This behavior suggests that the creation of Pd(111) domains is indeed responsible for the autocatalytic oxidation of CO on the √6 oxide. The peak at 1964 cm^{-1}, arising from bridging-CO on Pd(111), is the dominant feature in the RAIR spectra obtained after passing the rate maximum. The smaller features at 1895 and 2108 cm^{-1} are attributable to CO adsorbed in hollow and atop sites of Pd(111) facets, possibly in high-coverage compressed structures. Similar to the results obtained from the PdO(101) film, the appearance of a peak at 2001 cm^{-1} suggests that a fraction of the Pd atoms that are released from the √6 oxide organize into metallic (100) and/or (110)-like structures during reduction at 450 K.

Our results show that CO oxidation on both the √6 oxide and the multilayer PdO(101) film on Pd(111) occurs autocatalytically at 450 K, and that the PdO(101) film is intrinsically more reactive than the √6 oxide in the absence of O_2. The origin for the higher intrinsic reactivity of the PdO(101) surface vs. the √6 oxide is not exactly known, but may be caused, in part, by stronger binding of CO on PdO(101) compared with the √6 oxide. The autocatalytic reaction kinetics arises from the creation of reduced surface sites on which CO molecules bind more strongly compared with the pristine oxide surfaces. Our RAIRS data reveals that CO molecules attain significant concentrations on both O-vacancy sites of the PdO(101) surface and hollow sites of Pd(111) domains during reaction on the PdO(101) film at 450 K, and that the increase in CO oxidation rate during film reduction correlates with the presence of both Pd_{cus}/O_{cus} and Pd_{cus}/O_v sites. Our results also provide strong evidence that PdO(101) surface domains are efficiently regenerated during CO oxidation at 450 K as we find that PdO(101) surface sites are present on the surface even after ~3 ML of oxygen atoms (> four PdO(101) layers) are abstracted from the film.

In contrast to the PdO(101) results, the RAIRS data shows that CO molecules attain negligible concentrations on sites located within √6 oxide domains and only adsorb onto hollow sites of Pd(111) during reaction at 450 K and a CO partial pressure of 5×10^{-9} Torr. This finding indicates that O-vacancy sites are either not created on the √6 oxide surface or that such sites bind CO only weakly. The rapid increase in reaction rate that is observed as the √6 oxide is reduced is consistent with previous evidence[25, 33, 35] that high CO oxidation activity is achieved on late transition-metal surfaces when 2D oxide islands co-exist with metal domains. Compared with CO adsorbed on metallic domains that are spatially segregated from coexisting oxide domains, the adsorption of CO on O_v sites of PdO(101) provides CO molecules with more direct access to reactive sites within the PdO(101) domains (i.e., better mixing) which might enhance the reactivity of partially-reduced PdO(101) over that of a mixture of co-existing Pd(111) and √6 oxide domains. Overall, our results demonstrate that the PdO(101) surface is intrinsically more reactive than the √6 oxide toward CO oxidation in the absence of O_2, and that reaction creates oxygen vacancies within the PdO(101) surface domains that strongly bind CO molecules, leading to CO surface concentrations and reaction rates that increase as the oxide is reduced during reaction.

Acknowledgements

We acknowledge the Ohio Supercomputing Center for providing computational resources. We gratefully acknowledge financial support for this work provided by the Department of Energy, Office of Basic Energy Sciences, Catalysis Science Division through Grant DE-FG02-03ER15478.

References

1. J. F. Weaver, *Chem. Rev.*, 2013, **113**, 4164-4215.
2. H. Over, *Chem. Rev.*, 2012, **112**, 3356-3426.
3. H. Over, Y. D. Kim, A. P. Seitsonen, S. Wendt, E. Lundgren, M. Schmid, P. Varga, A. Morgante and G. Ertl, *Science*, 2000, **287**, 1474-1476.
4. M. D. Ackermann, T. M. Pedersen, B. L. M. Hendriksen, O. Robach, S. C. Bobaru, I. Popa, C. Quiros, H. Kim, B. Hammer, S. Ferrer and J. W. M. Frenken, *Phys. Rev. Lett.*, 2005, **95**, 255505.
5. P. A. Carlsson, V. P. Zhdanov and M. Skoglundh, *Phys. Chem. Chem. Phys.*, 2006, **8**, 2703-2706.
6. J. Gustafson, R. Westerström, A. Resta, A. Mikkelsen, J. N. Andersen, O. Balmes, X. Torrelles, M. Schmid, P. Varga, B. Hammer, G. Kresse, C. J. Baddeley and E. Lundgren, *Catal. Today*, 2009, **145**, 227-235.
7. M. A. Newton, A. J. Dent, S. Diaz-Moreno, S. G. Fiddy, B. Jyoti and J. Evans, *Chem. Eur. J*, 2006, **12**, 1975-1985.
8. H. Over, O. Balmes and E. Lundgren, *Catal. Today*, 2009, **145**, 236-242.
9. R. van Rijn, O. Balmes, A. Resta, D. Wermeille, R. Westerstrom, J. Gustafson, R. Felici, E. Lundgren and J. W. M. Frenken, *Phys. Chem. Chem. Phys.*, 2011, **13**, 13167-13171.
10. P. J. Berlowitz, C. H. F. Peden and D. W. Goodman, *J. Phys. Chem.*, 1988, **92**, 5213-5221.
11. D. W. Goodman, *Chem. Rev.*, 1995, **95**, 523-536.
12. J. A. Rodriguez and D. W. Goodman, *Surf. Sci. Rep.*, 1991, **14**, 1-107.
13. D. W. Goodman and C. H. F. Peden, *J. Phys. Chem.*, 1986, **90**, 4839-4843.
14. A. K. Santra and D. W. Goodman, *Electrochim. Acta*, 2002, **47**, 3595-3609.
15. J. Szanyi and D. W. Goodman, *J. Phys. Chem.*, 1994, **98**, 2972-2977.
16. J. Szanyi, W. K. Kuhn and D. W. Goodman, *J. Vac. Sci. Technol., A*, 1993, **11**, 1969-1974.
17. J. Szanyi, W. K. Kuhn and D. W. Goodman, *J. Phys. Chem.*, 1994, **98**, 2978-2981.
18. B. Hendriksen, S. Bobaru and J. Frenken, *Surf. Sci.*, 2004, **552**, 229-242.
19. J. Gustafson, M. Shipilin, C. Zhang, A. Stierle, U. Hejral, U. Ruett, O. Gutowski, P.-A. Carlsson, M. Skoglundh and E. Lundgren, *Science*, 2014, **343**, 758-761.
20. A. Farkas, K. Zalewska-Wierzbicka, C. Bachmann, J. Goritzka, D. Langsdorf, O. Balmes, J. Janek and H. Over, *J. Phys. Chem. C*, 2013, **117**, 9932-9942.
21. N. M. Martin, M. Van den Bossche, H. Grönbeck, C. Hakanoglu, J. Gustafson, S. Blomberg, M. A. Arman, A. Antony, R. Rai, A. Asthagiri, J. F. Weaver and E. Lundgren, *J. Phys. Chem. C*, 2013, **117**, 13510-13519.
22. Y. Jugnet, D. Loffreda, C. Dupont, F. Delbecq, E. Ehret, F. J. Cadete Santos Aires, B. S. Mun, F. Aksoy Akgul and Z. Liu, *J. Phys. Chem. Lett.*, 2012, **3**, 3707-3714.
23. R. Westerström, M. E. Messing, S. Blomberg, A. Hellman, H. Grönbeck, J. Gustafson, N. M. Martin, O. Balmes, R. van Rijn, J. N. Andersen, K. Deppert, H. Bluhm, Z. Liu, M. E. Grass, M. Hävecker and E. Lundgren, *Phys. Rev. B* 2011, **83**, 115440.
24. K. Zorn, S. Giorgio, E. Halwax, C. R. Henry, H. Grönbeck and G. n. Rupprechter, *J. Phys. Chem. C*, 2010, **115**, 1103-1111.
25. R. Westerström, J. G. Wang, M. D. Ackermann, J. Gustafson, A. Resta, A. Mikkelsen, J. N. Andersen, E. Lundgren, O. Balmes, X. Torrelles, J. W. M. Frenken and B. Hammer, *J. Phys.: Condens. Matter*, 2008, **20**, 184018.
26. E. Lundgren, A. Mikkelsen, J. N. Andersen, G. Kresse, M. Schmid and P. Varga, *J. Phys.: Condens. Matter*, 2006, **18**, R481.
27. S. Blomberg, M. J. Hoffmann, J. Gustafson, N. M. Martin, V. R. Fernandes, A. Borg, Z. Liu, R. Chang, S. Matera, K. Reuter and E. Lundgren, *Phys. Rev. Lett.*, 2013, **110**, 117601.

28. D. T. Vu, K. A. R. Mitchell, O. L. Warren and P. A. Thiel, *Surf. Sci.*, 1994, **318**, 129-138.
29. T. W. Orent and S. D. Bader, *Surf. Sci.*, 1982, **115**, 323-334.
30. R. Toyoshima, M. Yoshida, Y. Monya, K. Suzuki, B. S. Mun, K. Amemiya, K. Mase and H. Kondoh, *J. Phys. Chem. Lett.*, 2012, **3**, 3182-3187.
31. T. M. Pedersen, W. X. Li and B. Hammer, *Phys. Chem. Chem. Phys.*, 2006, **8**, 1566-1574.
32. E. Lundgren, J. Gustafson, A. Resta, J. Weissenrieder, A. Mikkelsen, J. N. Andersen, L. Köhler, G. Kresse, J. Klikovits, A. Biederman, M. Schmid and P. Varga, *J. Electron. Spectrosc. Relat. Phenom.*, 2005, **144–147**, 367-372.
33. H. Gabasch, A. Knop-Gericke, R. Schlogl, M. Borasio, C. Weilach, G. Rupprechter, S. Penner, B. Jenewein, K. Hayek and B. Klotzer, *Phys. Chem. Chem. Phys.*, 2007, **9**, 533-540.
34. D. Miller, H. Sanchez Casalongue, H. Bluhm, H. Ogasawara, A. Nilsson and S. Kaya, *J. Am. Chem. Soc.*, 2014, **136**, 6340-6347.
35. G. Zheng and E. I. Altman, *J. Phys. Chem. B*, 2002, **106**, 1048-1057.
36. A. L. Gerrard and J. F. Weaver, *J. Chem. Phys.*, 2005, **123**, 224703.
37. R. B. Shumbera, H. H. Kan and J. F. Weaver, *J. Phys. Chem. C*, 2008, **112**, 4232-4241.
38. J. F. Weaver, H. H. Kan and R. B. Shumbera, *J. Phys.: Condens. Matter*, 2008, **20**, 184015.
39. F. Gao and D. W. Goodman, *Langmuir*, 2010, **26**, 16540-16551.
40. J. A. Hinojosa, H. H. Kan and J. F. Weaver, *J. Phys. Chem. C*, 2008, **112**, 8324-8331.
41. J. T. Hirvi, T. J. J. Kinnunen, M. Suvanto, T. A. Pakkanen and J. K. Norskov, *J. Chem. Phys.*, 2010, **133**, 084704.
42. J. Klikovits, E. Napetschnig, M. Schmid, N. Seriani, O. Dubay, G. Kresse and P. Varga, *Phys. Rev. B* 2007, **76**, 045405.
43. G. Zheng and E. I. Altman, *Surf. Sci.*, 2000, **462**, 151-168.
44. E. Lundgren, G. Kresse, C. Klein, M. Borg, J. N. Andersen, M. De Santis, Y. Gauthier, C. Konvicka, M. Schmid and P. Varga, *Phys. Rev. Lett.*, 2002, **88**, 246103.
45. H. H. Kan, R. B. Shumbera and J. F. Weaver, *Surf. Sci.*, 2008, **602**, 1337-1346.
46. H. H. Kan and J. F. Weaver, *Surf. Sci.*, 2009, **603**, 2671-2682.
47. H. H. Kan and J. F. Weaver, *Surf. Sci.*, 2008, **602**, L53-L57.
48. G. Kresse and J. Furthmuller, *Phys. Rev. B*, 1996, **54**, 11169-11186.
49. G. Kresse and J. Hafner, *J. Non-Cryst. Solids*, 1993, **156**, 956-960.
50. P. E. Blöchl, *Phys. Rev. B*, 1994, **50**, 17953-17979.
51. G. Kresse and D. Joubert, *Phys. Rev. B*, 1999, **59**, 1758-1775.
52. J. P. Perdew, K. Burke and M. Ernzerhof, *Phys. Rev. Lett.*, 1996, **77**, 3865-3868.
53. J. F. Weaver, J. A. Hinojosa Jr, C. Hakanoglu, A. Antony, J. M. Hawkins and A. Asthagiri, *Catal. Today*, 2011, **160**, 213-227.
54. J. F. Weaver, C. Hakanoglu, J. M. Hawkins and A. Asthagiri, *J. Chem. Phys.*, 2010, **132**, 024709.
55. A. Antony, A. Asthagiri and J. F. Weaver, *Phys. Chem. Chem. Phys.*, 2012, **14**, 12202-12212.
56. A. Antony, C. Hakanoglu, A. Asthagiri and J. F. Weaver, *J. Chem. Phys.*, 2012, **136**, 054702.
57. J. A. Hinojosa, A. Antony, C. Hakanoglu, A. Asthagiri and J. F. Weaver, *J. Phys. Chem. C*, 2012, **116**, 3007-3016.
58. H. H. Kan, R. J. Colmyer, A. Asthagiri and J. F. Weaver, *J. Phys. Chem. C*, 2009, **113**, 1495-1506.
59. C. Hakanoglu, J. M. Hawkins, A. Asthagiri and J. F. Weaver, *J. Phys. Chem. C*, 2010, **114**, 11485-11497.
60. N. M. Martin, M. Van den Bossche, H. Grönbeck, C. Hakanoglu, F. Zhang, T. Li, J. Gustafson, J. F. Weaver and E. Lundgren, *J. Phys. Chem. C*, 2013, **118**, 1118-1128.
61. A. Farkas, G. C. Mellau and H. Over, *J. Phys. Chem. C*, 2009, **113**, 14341-14355.
62. A. Farkas, F. Hess and H. Over, *J. Phys. Chem. C*, 2012, **116**, 581-591.

63. K. Wolter, O. Seiferth, H. Kuhlenbeck, M. Baumer and H. J. Freund, *Surf. Sci.*, 1998, **399**, 190-198.
64. F. Gao, Y. Wang, Y. Cai and D. W. Goodman, *J. Phys. Chem. C*, 2008, **113**, 174-181.
65. H. Ohtani, M. A. V. Hove and G. A. Somorjai, *Surf. Sci.*, 1987, **187**, 372-386.
66. G. Ertl and J. Koch, *Z. Naturforsch. Pt. A*, 1970, **A 25**, 1906.
67. F. M. Hoffmann, *Surf. Sci. Rep.*, 1983, **3**, 107-192.
68. A. Ortega, F. M. Hoffman and A. M. Bradshaw, *Surf. Sci.*, 1982, **119**, 79-94.
69. R. Raval, M. A. Harrison and D. A. King, *Surf. Sci.*, 1989, **211–212**, 61-70.
70. T. M. Pedersen, W. Xue Li and B. Hammer, *Phys. Chem. Chem. Phys.*, 2006, **8**, 1566-1574.
71. M. Hoffmann and K. Reuter, *Top. Catal.*, 2014, **57**, 159-170.
72. J. Rogal, K. Reuter and M. Scheffler, *Phys. Rev. B*, 2008, **77**, 155410.
73. J. Rogal, K. Reuter and M. Scheffler, *Phys. Rev. Lett.*, 2007, **98**, 046101.
74. J. Rogal, K. Reuter and M. Scheffler, *Phys. Rev. B* 2007, **75**, 205433.

Figure Captions

Figure 1 Model representations of the (a) √6 surface oxide (Pd_5O_4) on Pd(111) and (b) PdO(101) in which Pd and O atoms are colored blue and red, respectively. The square (√6 × √6) unit cell of the Pd_5O_4 surface oxide is given by dashed lines while the larger coincident unit cell is drawn in black. The bridge-A, atop 2f and bridge-B sites, discussed in the text, are marked with the numbers 1, 2 and 3, respectively.

Figure 2 CO_2 production rate vs. time measured during CO oxidation (5×10^{-9} Torr) at 450 K on O-covered Pd(111) (black), the √6 oxide (red) and a PdO(101) film (blue) grown on Pd(111). The initial oxygen coverages are 0.21 ML, 0.70 ML and 3.50 ML.

Figure 3 Reaction (a) and resaturation IR spectra (b) of CO obtained after each 5-minute reaction interval on PdO(101) at 450 K. The estimated cumulative time at which CO oxidation occurred on the surface at 450 K is listed above each spectrum. The bottom spectrum in (b) is the reference for CO adsorbed to saturation on PdO(101) at 95 K. The spectrum marked with "*" was obtained shortly after the maximum rate of isothermal reaction. All IR spectra were collected at 95 K.

Figure 4 Reaction (a) and resaturation IR spectra (b) of CO during and after each 3-minute reaction interval on √6 oxide at 450 K. The estimated cumulative time at which CO oxidation occurred on the surface at 450 K is listed above each spectrum. The bottom spectrum in (b) is the reference for CO adsorbed to saturation on the √6 oxide at 95 K. The spectrum marked with "*" was obtained shortly after the maximum rate of isothermal reaction. All IR spectra were collected at 95 K.

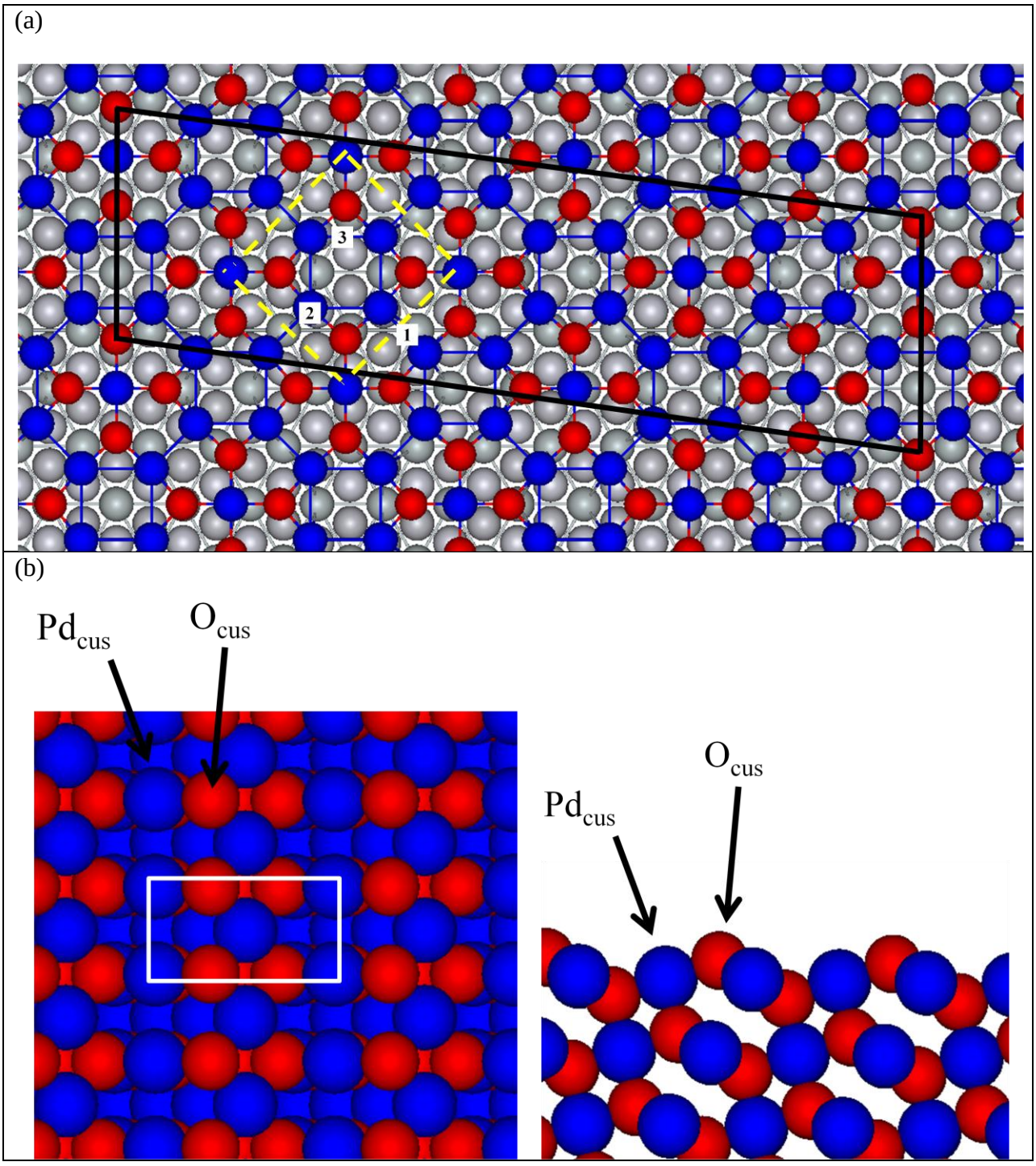

Figure 1 Zhang et al.

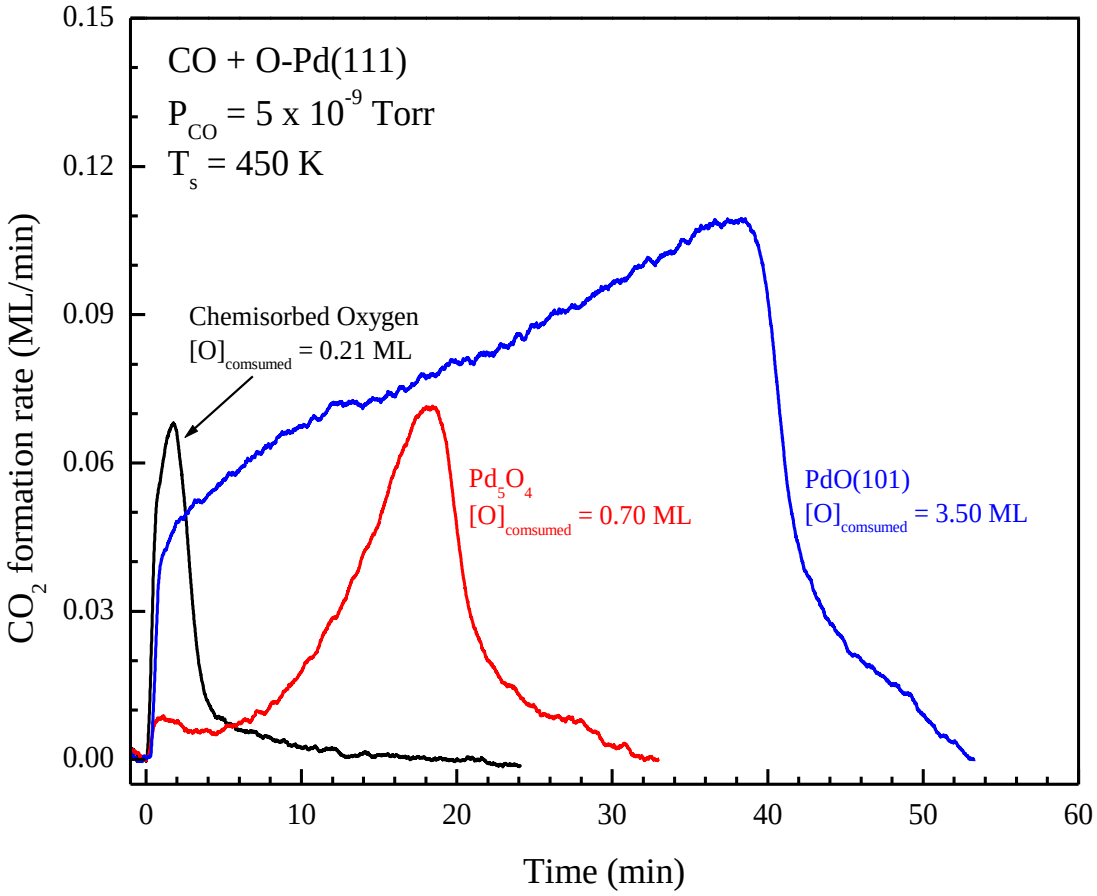

Figure 2 Zhang et al.

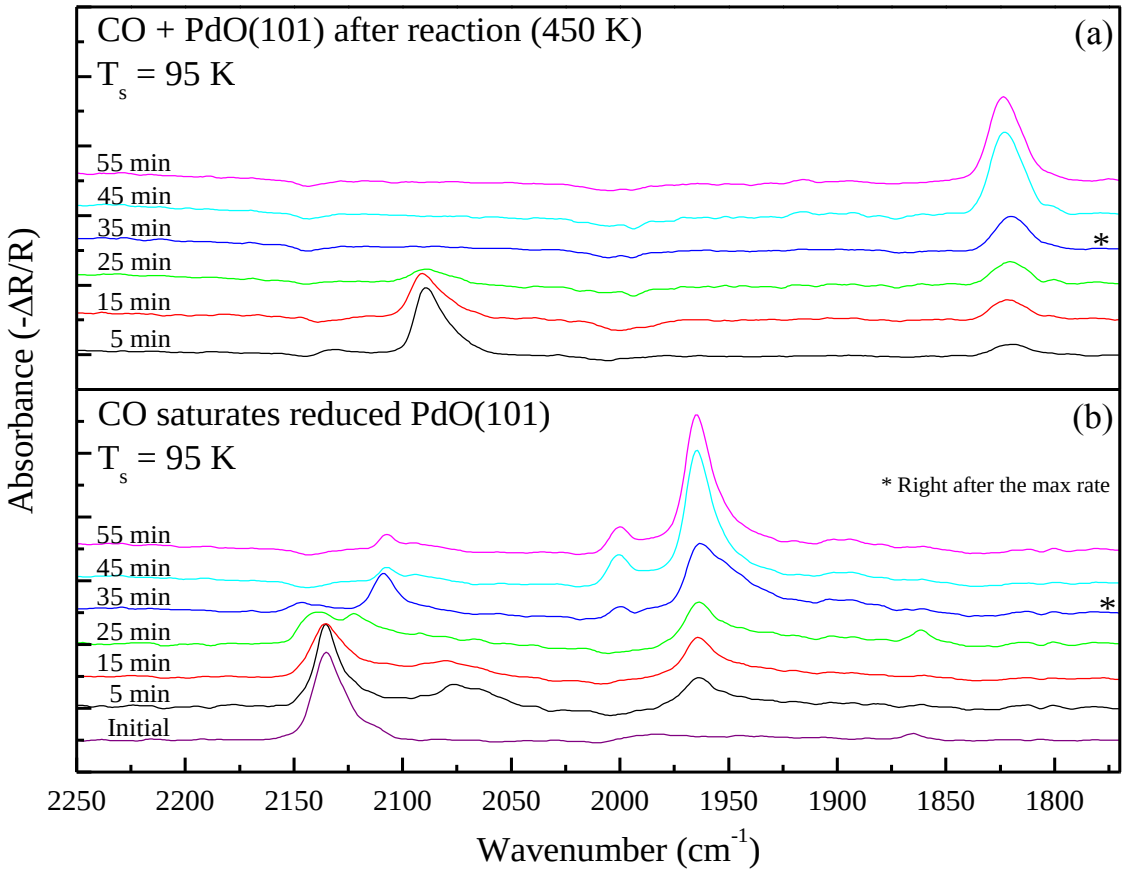

Figure 3

Zhang et al.

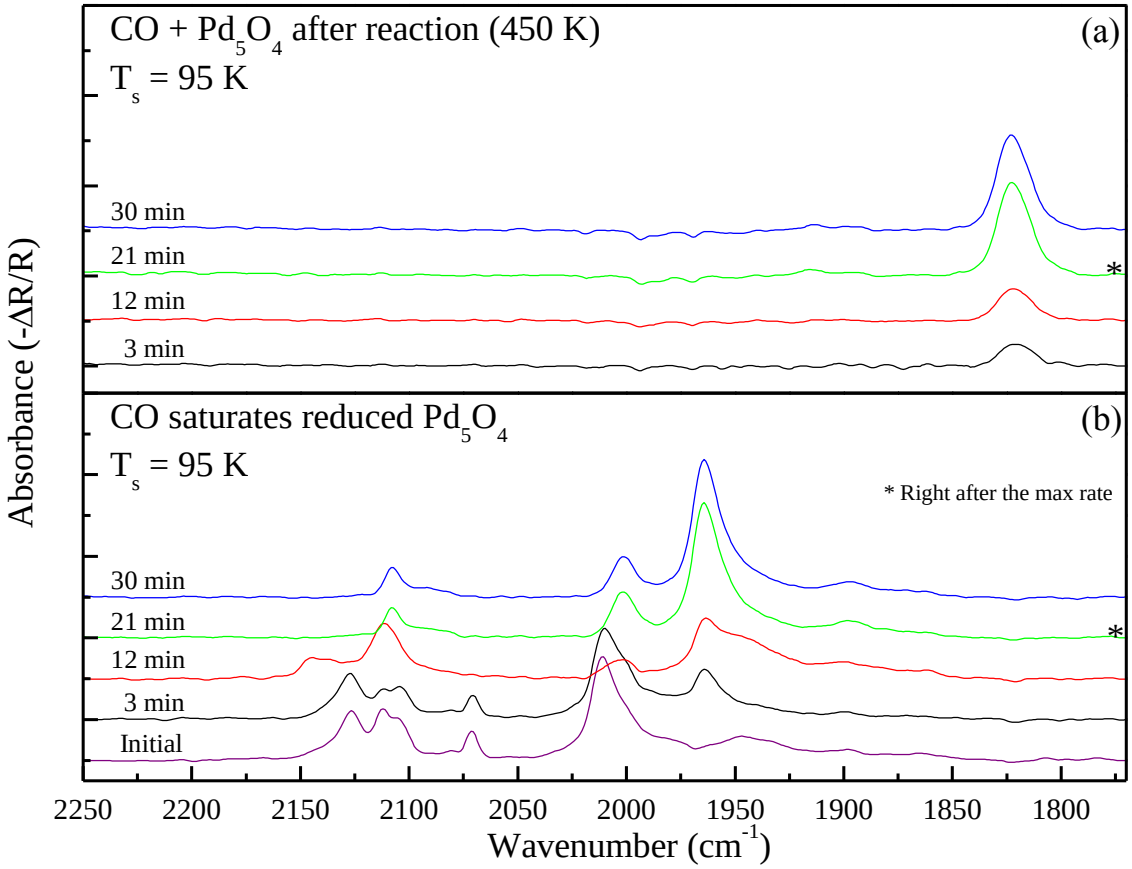

Figure 4 Zhang et al.